Electronic Supporting Information

to

Highly stable silver nanohybrid electrocatalysts for oxygen reduction reaction

Quentin Lenne,[a] Maurice Retout,[b] Bryan Gosselin,[b] Gilles Bruylants,[b] Ivan Jabin,[c] Jonathan Hamon,[d] Corinne Lagrost,*[,a] Yann Leroux*[,a]

[a] Univ. Rennes, CNRS, ISCR – UMR 6226, 35000 Rennes, France.

[b] EMNS, Université libre de Bruxelles (ULB), avenue F. D. Roosevelt 50, CP165/64, B-1050 Brussels, Belgium.

[c] LCO, Université libre de Bruxelles (ULB), CP 160/06, avenue F.D. Roosevelt 50, 1050 Brussels, Belgium.

[d] IMN, 2 rue de la Houssinière, 44000 Nantes, France.

Table of contents

1. General Information.

Chemicals. Solvents and reagents for the electrochemical analysis were ultra-pure with no trace metals and purchased from Sigam-Aldrich. Nafion 117® has been purchased from Sigma-Aldrich. The commercial citrates capped silver nanoparticles were purchased from Clinisciences.

Electronic absorption spectra. The electronic absorption spectra was recorded with a Shimadzu UV1605 spectrophotometer.

IR spectroscopy. The diffusion powder spectra of the calix-AgNPs were recorded with a Jasco FT/IR-4600 spectrometer**.**

Transmission Electron Microscopy. Morphology and size distribution of the samples were investigated by high-resolution transmission electron microscopy (HRTEM), using a Jeol 2100 with an acceleration voltage of 200 kV on which the images were recorded on a GATAN Orius 200 CCD camera. The size distribution was estimated using ImageJ software, version 1.52a.

X-ray photoelectron spectroscopy measurements. XPS data have been collected by a Kratos Axis Nova spectrometer using the Al Kα X-ray source working at 1486.6 eV and using a spot size of 0.7 x 0.3 mm². Survey spectra (0-1000 eV) were acquired with an analyzer pass energy of 160 eV (0.5 eV/step); high resolution spectra used a pass energy of 40 eV (0.1 eV/step). Binding energies were referenced to C1s peak at 285 eV. The core level spectra were peak-fitted using the CasaXPS Software, Ltd. Version 2.3.18. U2 Tougaard was used as background. The peaks areas were normalized by the manufacturer-supplied sensitivity factor (S_{C1s} = 0.278, S_{F1s} = 1, S_{O1s} = 0.78, S_{S2p} = 0.668, S_{Au4f} = 6.25). Since the XPS measurements cannot be made with the RRDE electrodes due to their height, deposit of AuNPs were performed onto screen-printed carbon electrode Dropsens®. The modified electrodes subsequently underwent ORR stability experiments (1000 cycles at 500mV.s^{-1} from 1.20V to -0.35V vs RHE) under the same experimental conditions used for ORR measurements with RRDE. For each sample, XPS spectra were recorded on three different locations, and we did not observe any difference.

Electrochemical measurements. The ORR activity was evaluated using a rotating Pt/GC ring-disk electrode (37% collection efficiency) controlled by a MSR Rotator from Pine Research. The LSV scans were recorded using an Autolab PGSTAT302N potentiostat-galvanostat (Metrohm) equipped with a BIPOT module, in a conventional three-electrode electrochemical cell at a scan rate of 10 $mV.s^{-1}$ in a 0.1 M KOH solution saturated with O_2. A graphite rod and a Hg/HgO, KOH (20%) electrode were used as counter and reference electrodes, respectively. Voltammograms were recorded with the Metrohm Nova 1.11 software. The potentials were not corrected from iR-drop. The potentials are reported against the reversible hydrogen electrode according to E (RHE) = E (Hg/HgO) + 0.059 pH + 0.140. The onset potential E_{onset} was determined on the LSV curves as the potential corresponding to 5/100 of I_L, I_L being the diffusion limiting current.

Synthesis of calix[4]arene-tetraacetic acid-tetradiazonium salt X4. The synthesis of compound **X4** was achieved in five steps from commercially available *p-t*Bu-calix[4]arene. First, the tetra-amino derivative was obtained according to the literature.[1] Note however that the reduction of the nitro groups of the intermediate tetra-nitro derivative was achieved through hydrogenation (H_2, Pd/C) and not by using $SnCl_2$, as it was previously described. Compound **X4** was then prepared from the tetra-amino derivative following a previously described procedure.[2]

2. Synthesis and characterization of calix-AgNPs.

The synthesis of the two series of calix-AgNPs is adapted from reference [3]:
1 mL of $AgNO_3$ aqueous solution (2 mM) is added to 1 mL of an aqueous solution containing calix[4]arene-tetra-diazonium salt **X4** (2.4 mM). The pH of the solution is adjusted to 7 by the addition of NaOH (1M). The solution is stirred and heated to 60°C before 0.5 mL of an aqueous solution containing $NaBH_4$ (8 mM) or sodium ascorbate (8 mM) is added to obtain 6 nm and 18 nm calix-AgNPs respectively. The solution is finally stirred 16 h at 60°C. At the end of the reaction, the nanoparticles were washed four times through centrifugation.

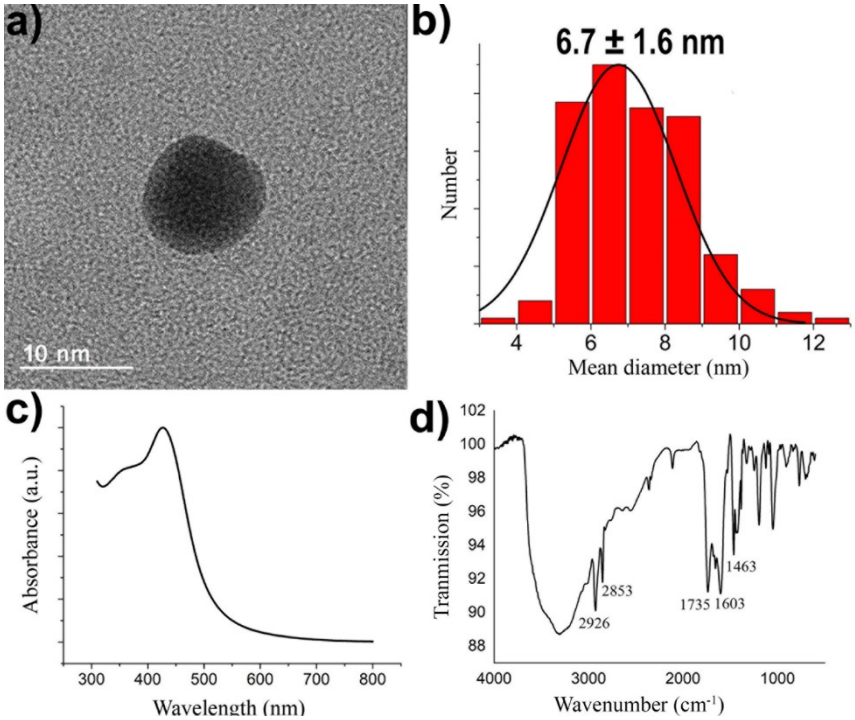

Figure S1. (a) TEM micrograph and (b) its corresponding distribution histogram, (c) UV-Vis absorption and (d) diffusion powder IR spectrum of 6 nm calix-AgNPs.

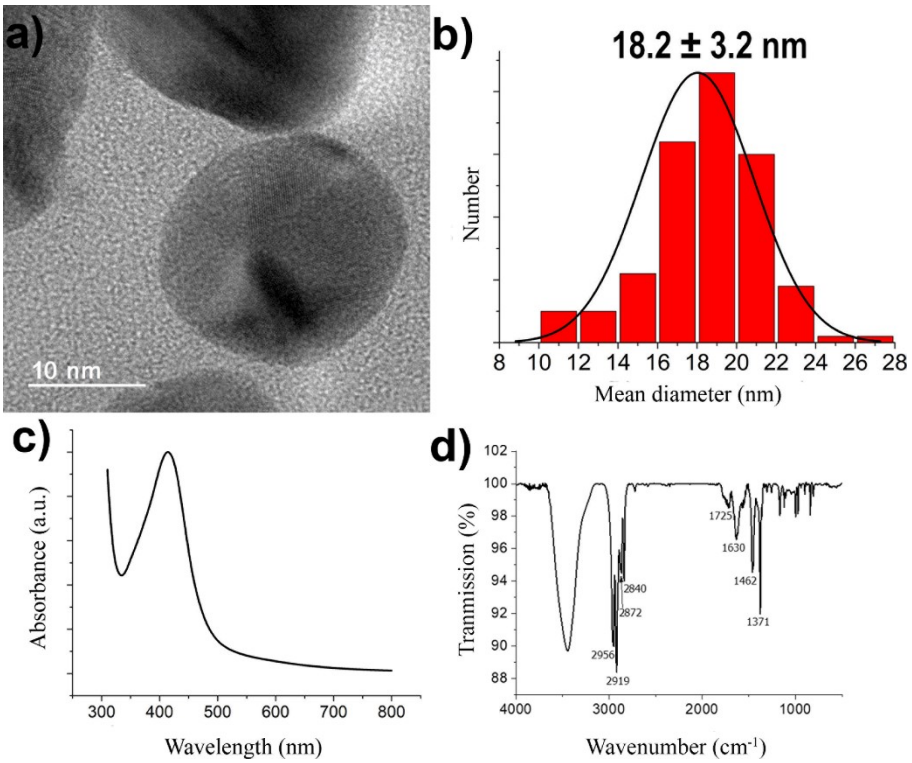

Figure S2. (a) TEM micrograph and (b) its corresponding distribution histogram, (c) UV-Vis absorption and (d) powder diffusion IR spectrum of 18 nm calix-AgNPs.

The characteristic IR bands of the calix[4]arene-tetraacetic acid-tetra-aniline precursors used in this study were determined to be at 3368, 2940, 1611, 1480 and 1225 cm^{-1}.[1] Similar characteristic IR bands can be observed at 2926, 1603 and 1463 cm^{-1} for 6 nm calix-AgNPs and 2956, 1630 and 1462 cm^{-1} for 18 nm calix-AgNPs.

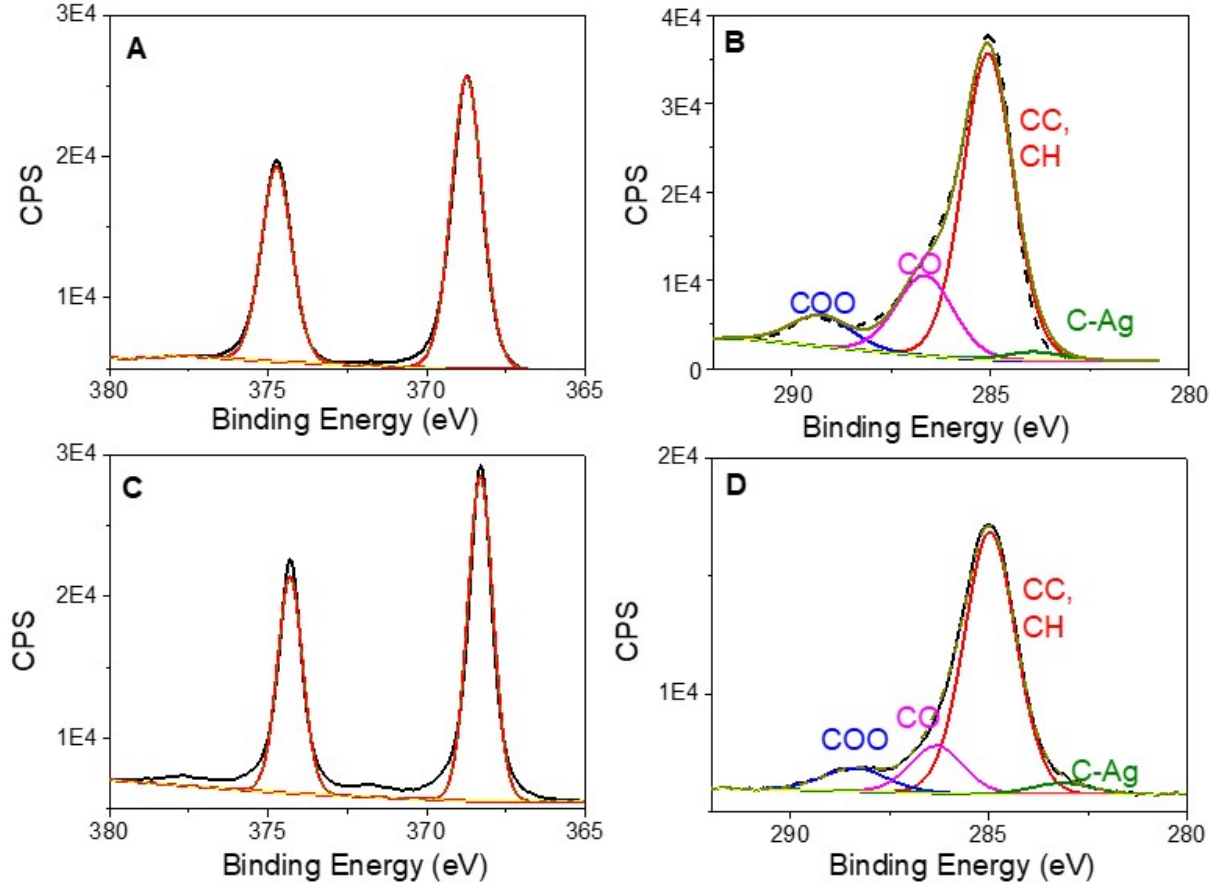

Figure S3. High resolution XPS core level spectra of the Ag 3d (A, C) and of the C 1s (B, D) regions for deposits of calix-AgNPs of 6 nm (A, B) and 18 nm (C, D) onto Si substrates.

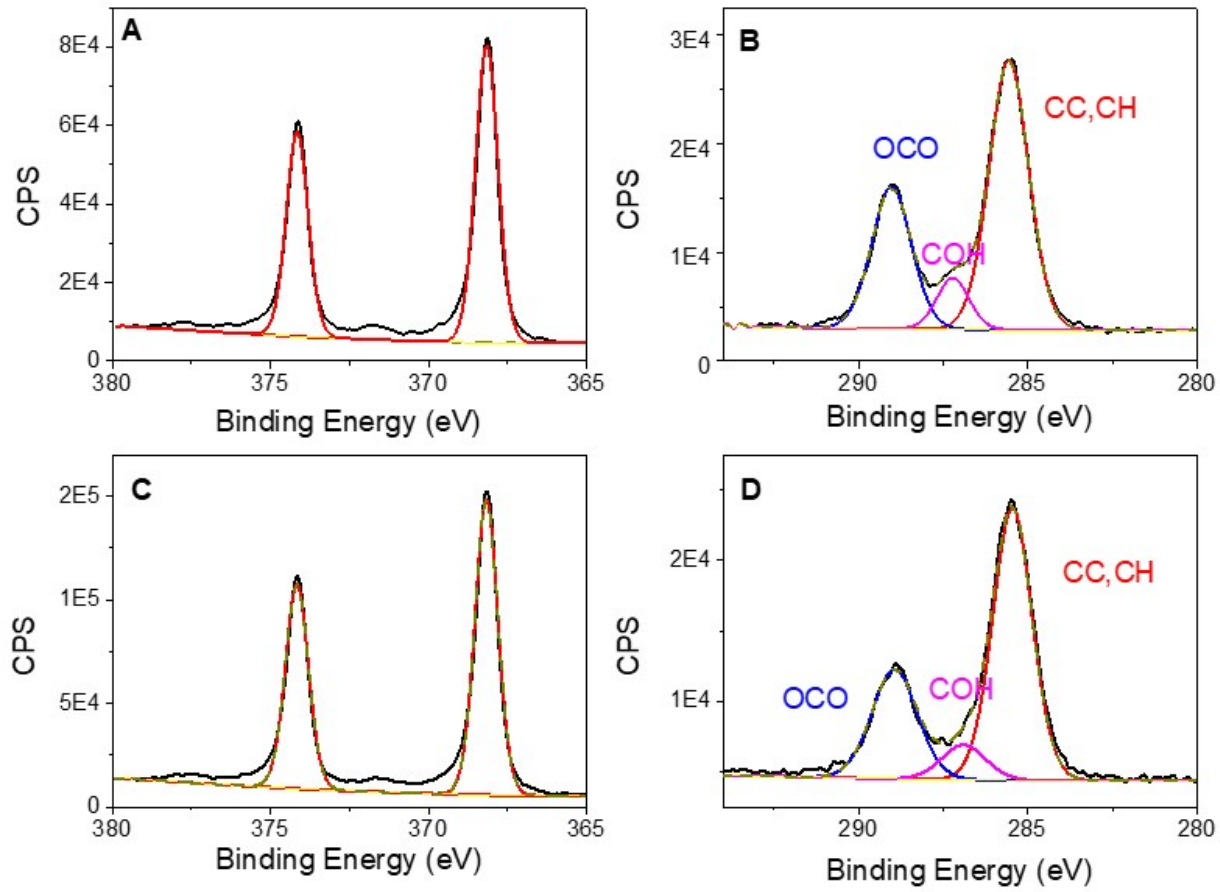

Figure S4. High resolution XPS core level spectra of the Ag 3d (A, C) and of the C 1s (B, D) regions for deposits of citrate-AgNPs of 5 nm (A, B) and 20 nm (C, D) onto Si substrates.

The Ag 3d XPS signal presents a pair of peaks corresponding to Ag 3d3/2 and Ag 3d5/2. The Ag 3d5/2 peaks were located at 368.7 eV, 368.3 eV, 368.1 eV and 368.1 eV for calix-AgNPs of 6 nm, calix-AgNPs of 18 nm, citrate-AgNPs of 5 nm and citrate-AgNPs of 20 nm, respectively. (Figures S3 A-C, Figures S4 A-C). Such values would be in agreement with metallic Ag^0. However, it is well known that determination of chemical states using XPS spectroscopy is especially difficult because shift in electronic binding energies could be comparable or even less to that of instrument resolution. To overcome such an issue, the calculation of modified Auger parameter (α') derived from thesum of the binding energy of Ag 3d5/2 photoemission peak with the kinetic energy of the sharpest $M_4N_{45}N_{45}$ Auger lineleads to the chemical state of the silver nanoparticles with a better accuracy while being not sensitive to charging effect.[4, 5] We determined $\alpha' \geq 726$ eV for all the NPs, indicating their metallic character.[4-6]

The C 1s signal in figures S3 B,D could be decomposed into 3 main components attributed to CC, CH (285 eV), CO (286.5 and 286.3eV), COO (288.7 and 289.3 eV) groups. The atomic ratio CO/COO is equal to 2.4, close to the theoretical value of 2 for the calix[4]arene structure having 4 ether and 4 carboxylate functions. Similarly, the C1s signal for citrate-AgNPs is decomposed into 3 components corresponding to the CC, CH (285.5 and 285.4 eV), COH (287.2 and 286.9 eV) and COO^- (289.0 and 288.95 eV) functions in the citrate molecules (Figure S4 B, D). The ratio COH/COO^- is equal to 0.29 and 0.31 respectively for citrate-AgNPs 5 and 20 nm, respectively in agreement with the expected 0.33 value with respect to the citrate structure.

3. Electrode preparation.

Prior to use, the GC disk (5 mm of diameter)/Pt ring electrode (Pine research) was polished with alumina suspension (0.3 µm, Struers) to obtain a mirror-like surface. It was then extensively rinsed with isopropanol and immersed in milli-Q water (18.2 MΩ) under sonication for 10 min. The electrode is finally dried under a stream of Argon. 40µL of AgNPs solutions were dropped onto the GC surface. 10 µL of 0.5% Nafion 117® (Sigma Aldrich) solution was pipetted onto the AgNPs deposit to ensure mechanical stability of the deposits.

4. RRDE analyses of 18 nm calix-AgNPs and 20 nm citrate-AgNPs.

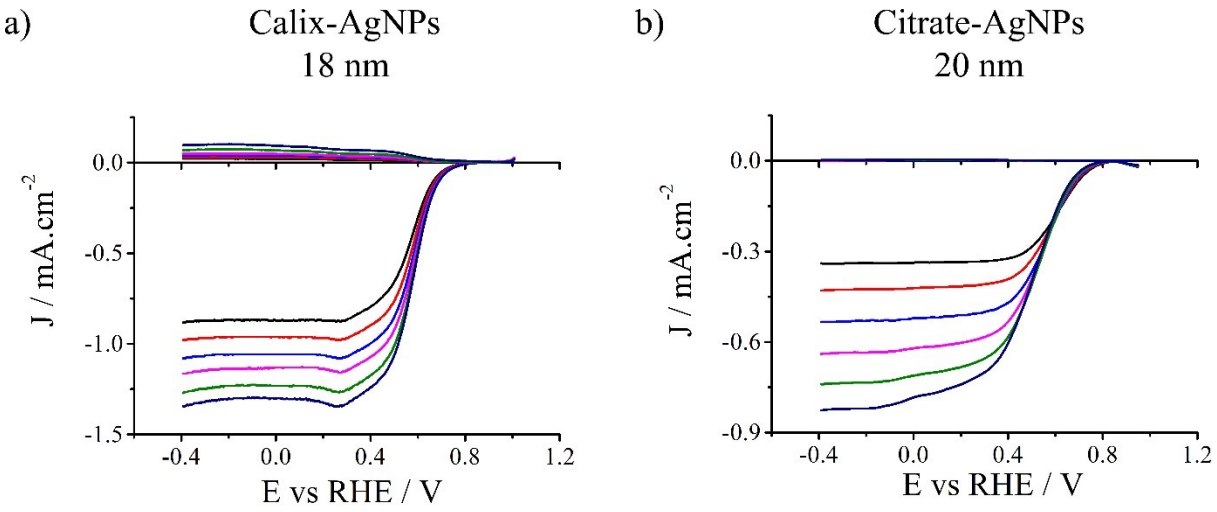

Figure S5. RRDE voltammetric curves in O_2-saturated 0.1 M KOH of GC disk electrodes modified with either a) 18 nm calix-AgNPs or b) 20 nm citrate-AgNPs (bottom curves). Ring electrode (top curves): Pt. v = 10 mV.s^{-1}, 400 rpm < ω < 2000 rpm, E_{ring} = 1.70 V vs RHE.

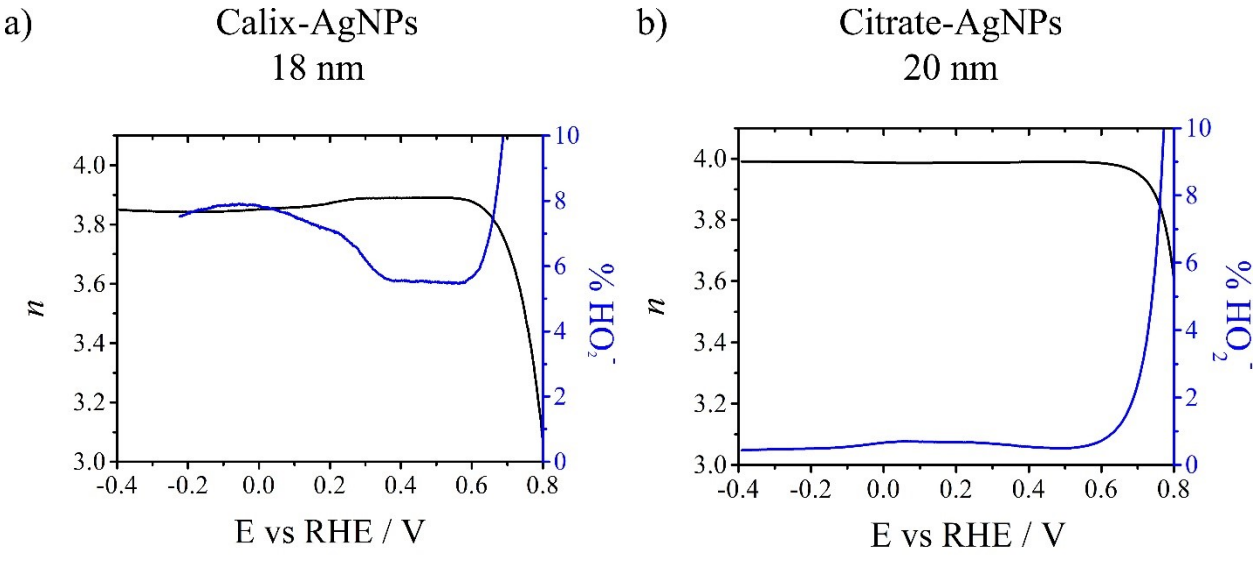

Figure S6. Potential dependence of the number of electrons *n* (black lines) and the proportion of HO_2^- (blue lines) produced during ORR experiments for a) 18 nm calix-AgNPs and b) 20 nm citrate-AgNPs.

5. Measurements of the Electrochemically Active Surface Area (ECSA).

As pointed out in the literature, the ECSA of Ag nanostructures remains difficult to determine with high accuracy,[7] but three methods could be envisaged: underpotential deposition of Pb,[8] integration of the cyclic voltammogram peak associated with Ag to Ag_2O oxidation[9] or from the double layer capacitance.[10] We decided to use the last method for two reasons: i) Campbell and Compton have clearly demonstrated that the distinct features of Pb_{upd} were diminished onto small nanoparticles and may be due to alloy formation at the nanoscale,[8] and ii) the oxidation of Ag is known to be only partially reversible, hence eventually impacting the measured electrocatalytic activity of the NPs after ECSA measurements. Table S1 summarizes the results obtained on both calix-AgNPs and citrate-AgNPs.

Table S1. Electrochemically active surface area (ECSA) of AgNPs before and after stability tests in 1 M KOH solution.

	ECSA before stability tests (cm^2)	ECA after stability tests (cm^2)	% loss
Calix-AgNPs 6 nm	0.29	0.16	44 %
Calix-AgNPs 18 nm	0.44	0.25	43 %
Citrate-AgNPs 5 nm	4.09	0.65	84 %
Citrate-AgNPs 20 nm	1.81	0.11	94 %

6. Mass-transfer corrected Tafel plots.

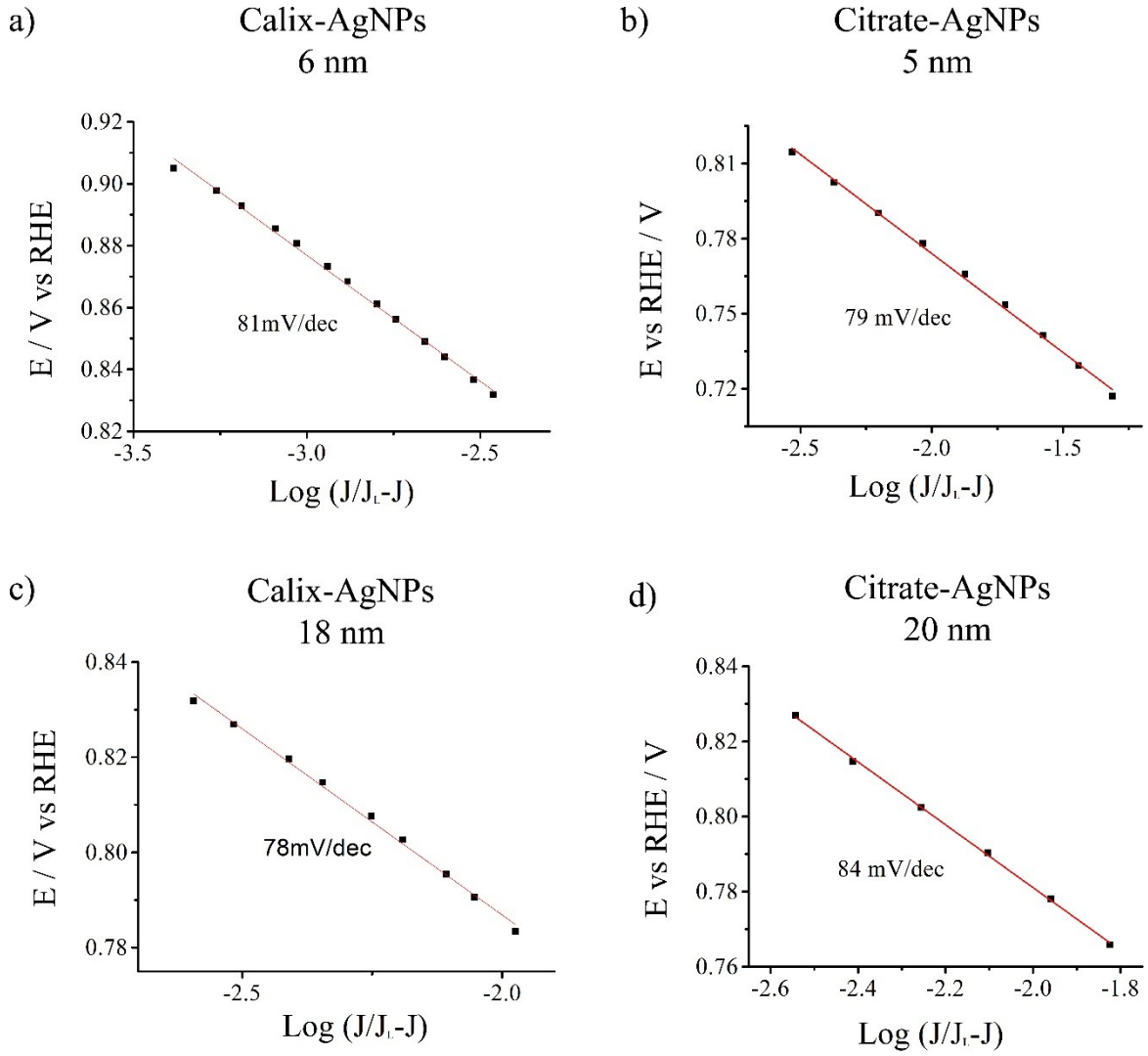

Figure S7. Mass-transfer corrected Tafel plots for O_2 reduction for a) 6 nm calix-AgNPs and b) 5 nm citrate-AgNPs, c) 18 nm calix-AgNPs and d) 20 nm citrate-AgNPs in O_2-saturated aqueous 0.1 M KOH solution. v =10 mV.s^{-1}; ω = 1600 rpm.

7. Stability test for calix-AgNPs and citrate-AgNPs.

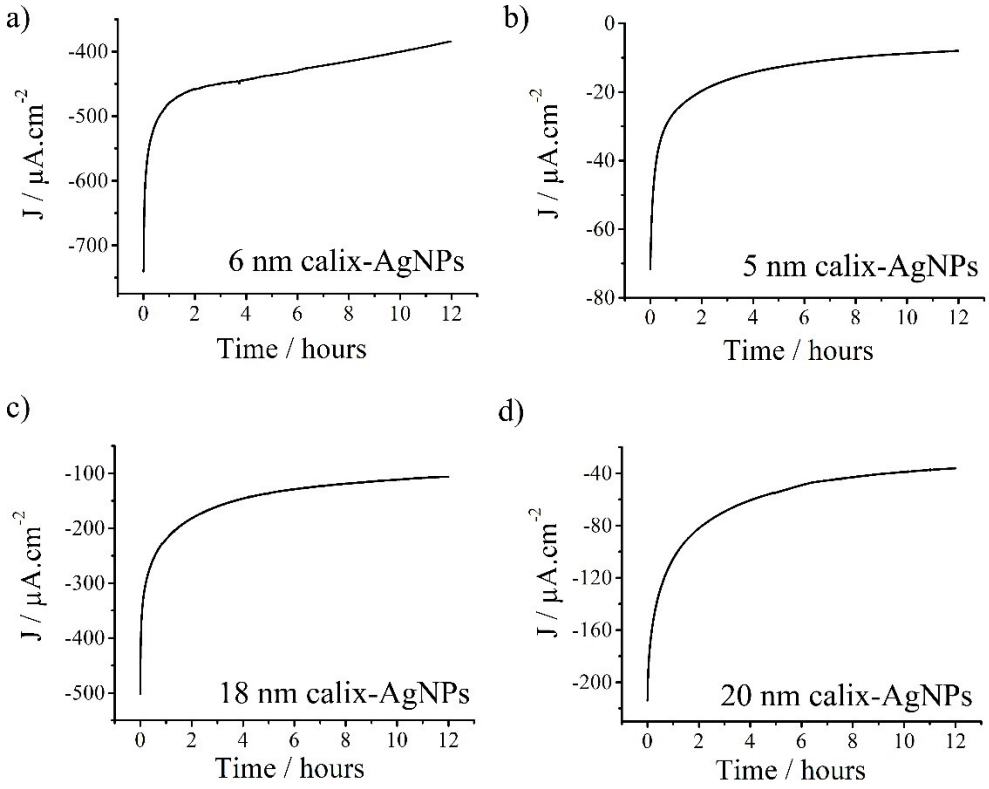

Figure S8. 12 hours chronoamperometry curves of a) 6 nm calix-AgNPs, b) 5 nm citrates-AgNPs, c) 18 nm calix-AgNPs and d) 20 nm citrates-AgNPs recorded at 900 rpm at 0.55 V vs. RHE in O_2 saturated 0.1 M KOH solution.

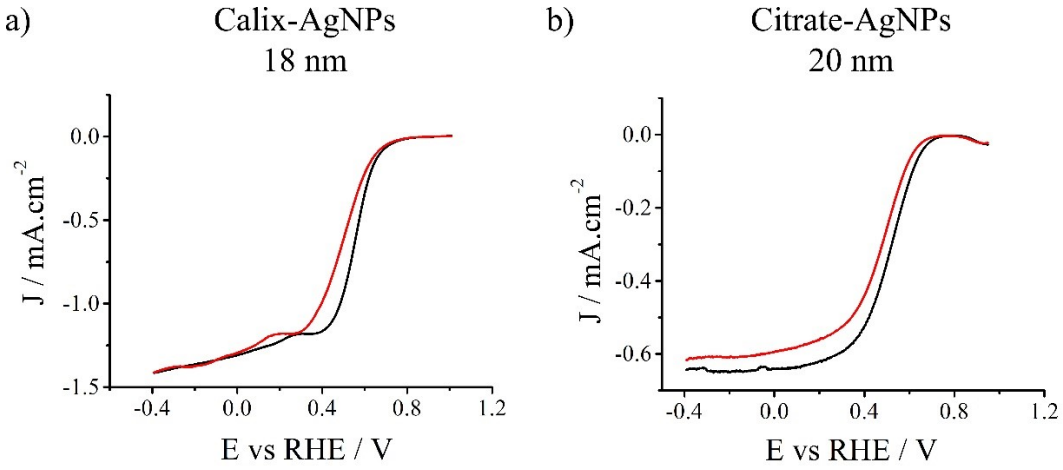

Figure S9. Linear sweep voltammetry (LSV) curves recorded at 1600 rpm on a) 18 nm calix-AgNPs and b) 20 nm citrates-AgNPs before (black lines) and after (red lines) chronoamperometry in O_2-saturated 0.1 M KOH solution.

8. XPS analyses before and after stability tests.

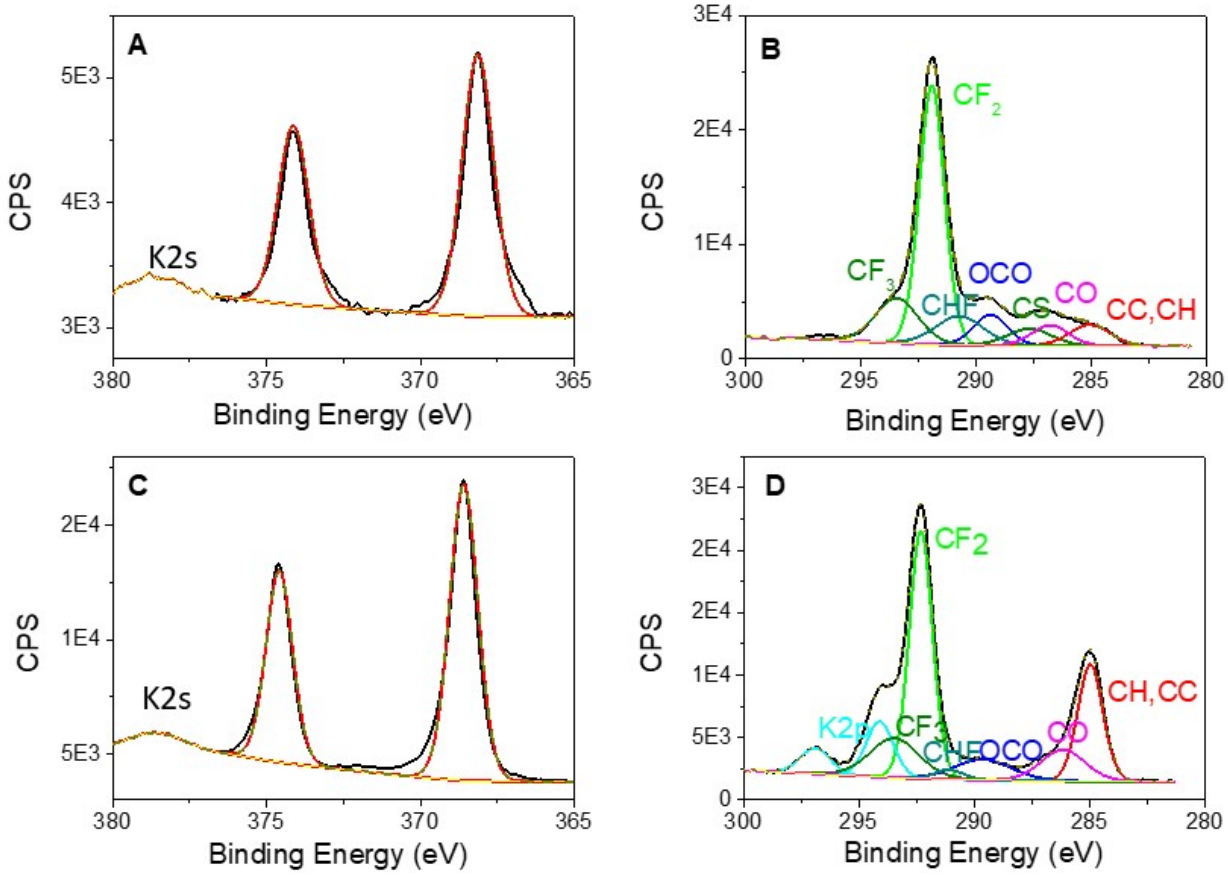

Figure S10. High resolution XPS core level spectra of the Ag 3d (A, C) and of the C 1s (B, D) regions for deposits of 6 nm calix-AgNPs before (A, B) and after (C, D) accelerated durability test (ADT).

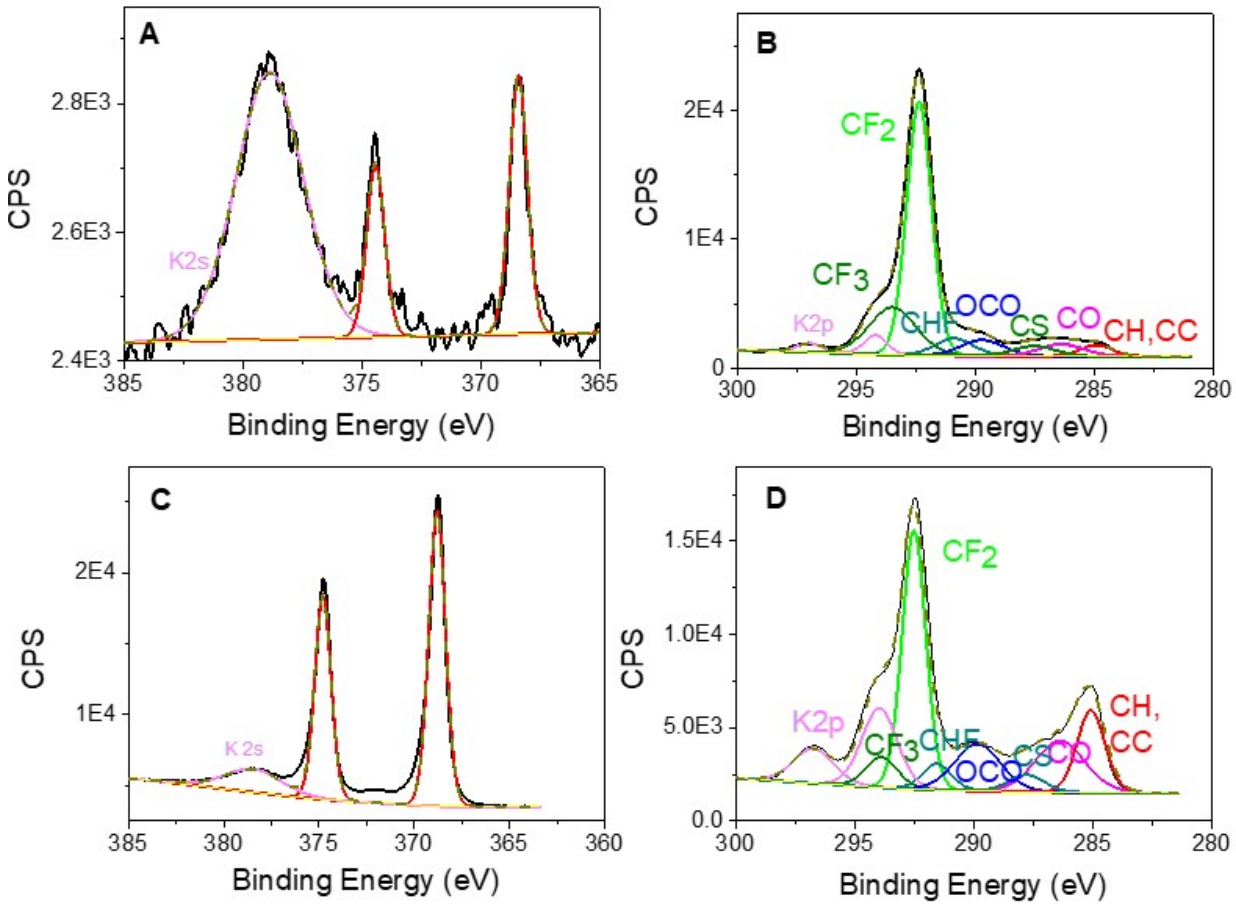

Figure S11. High resolution XPS core level spectra of the Ag 3d (A, C) and of the C 1s (B, D) regions for deposits of 18 nm calix-AgNPs before (A, B) and after (C, D) accelerated durability test (ADT).

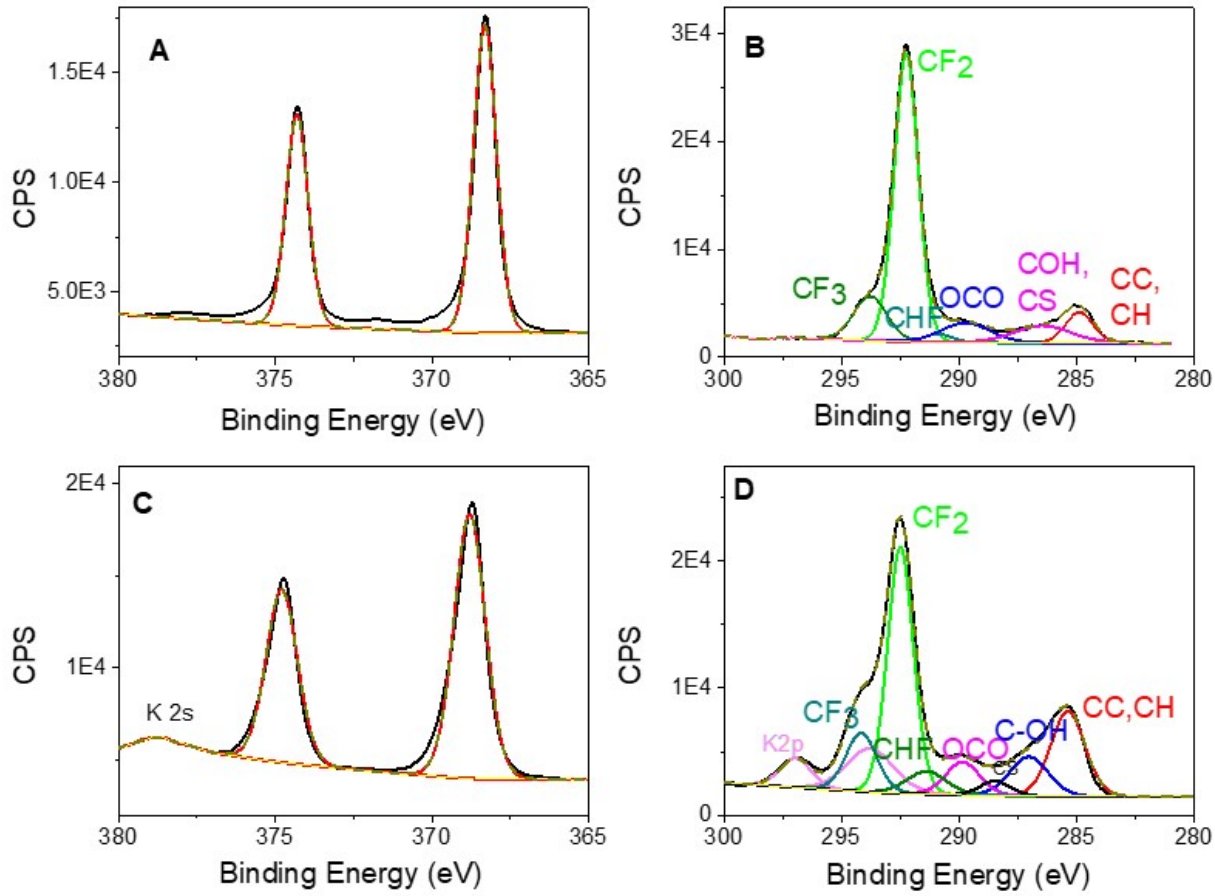

Figure S12. High resolution XPS core level spectra of the Ag 3d (A, C) and of the C 1s (B, D) regions for deposits of 5 nm citrate-AgNPs before (A, B) and after (C, D) accelerated durability test (ADT).

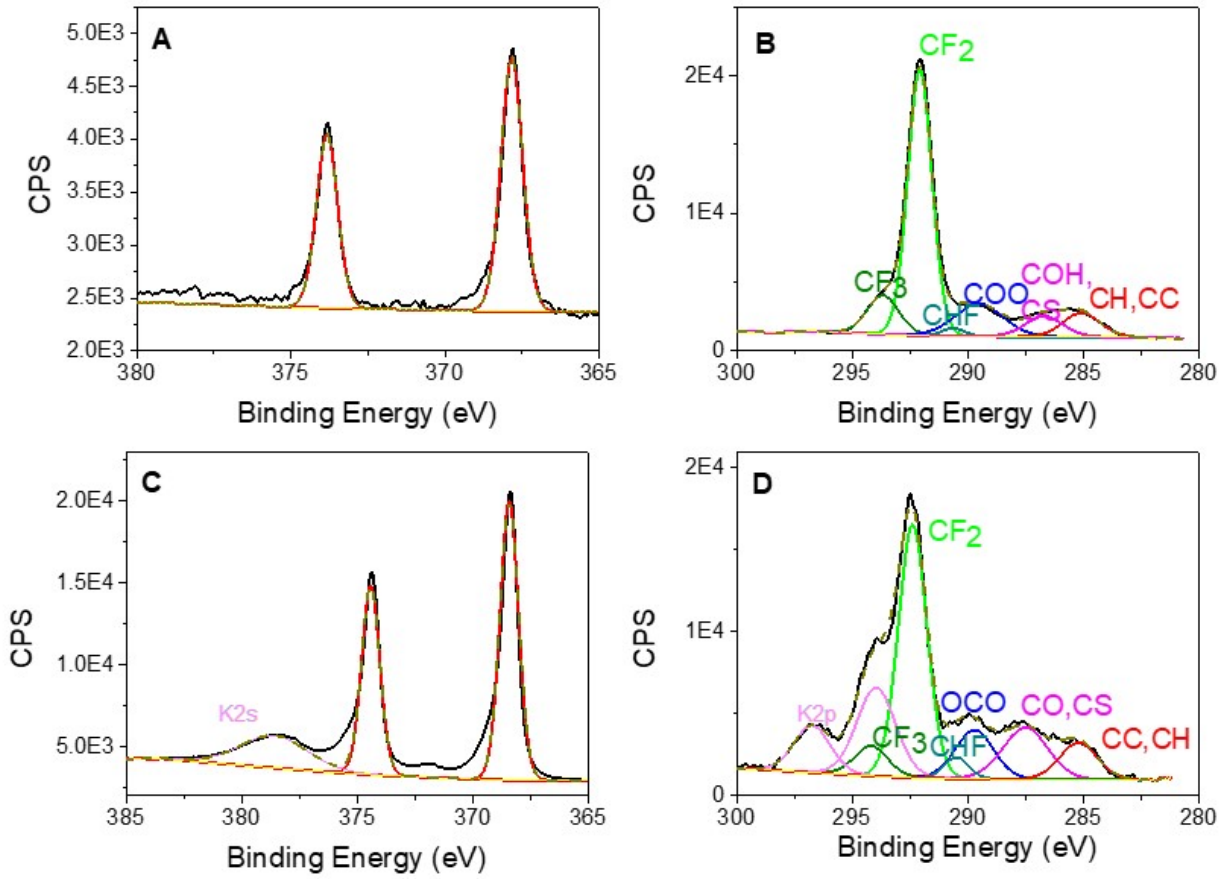

Figure S13. High resolution XPS core level spectra of the Ag 3d (A, C) and of the C 1s (B, D) regions for deposits of 20 nm citrate-AgNPs before (A, B) and after (C, D) accelerated durability test (ADT).

The C1s signals show strong contributions due to Nafion (figures S10, 11, 12, 13 B and D). Presence of potassium is also noticeable after ADT for all series of Ag nanoparticles because the treatment is achieved in KOH but also for calix-AgNPs before ADT because the nanoparticles were stored in a 0.1 M KOH solution. After durability tests, the modified Auger parameters α' are equal to 726.2 and 726.25 eV for the calix-AgNPs 6 and 18 nm, respectively. Such values indicate that the nanoparticles retain their metallic character after ORR operation. In sharp contrast, α' are found equal to 724.6 and 725.9 eV for citrate-AgNPs 5 and 20 nm. They clearly show that the Ag nanoparticles are oxidized under ORR operation, at least partially for citrate-Ag NPs 20 nm. Indeed, these α' values are characteristic of silver oxides.[4-6] Interestingly, the smallest citrate Ag-NPs appeared much more sensitive to oxidation than their largest counterparts.

9. Methanol tolerance.

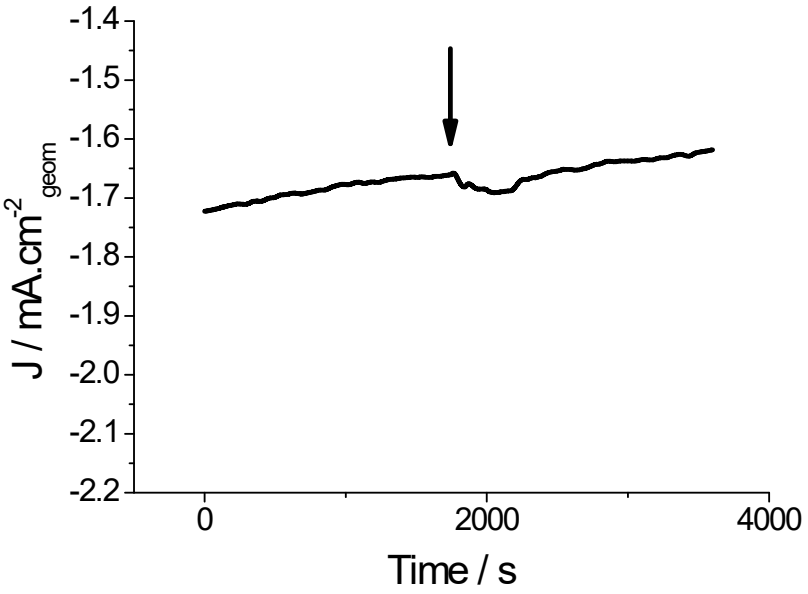

Figure S14. Chronoamperometric curve of calix-AgNPs (6 nm) in O_2 saturated 0.1 M KOH solution with addition of 3 M methanol (addition performed at time shown by the arrow) at 0.55 V vs RHE at 1600 rpm.

10. Comparison of silver electrocatalysts and Pt/C for ORR.

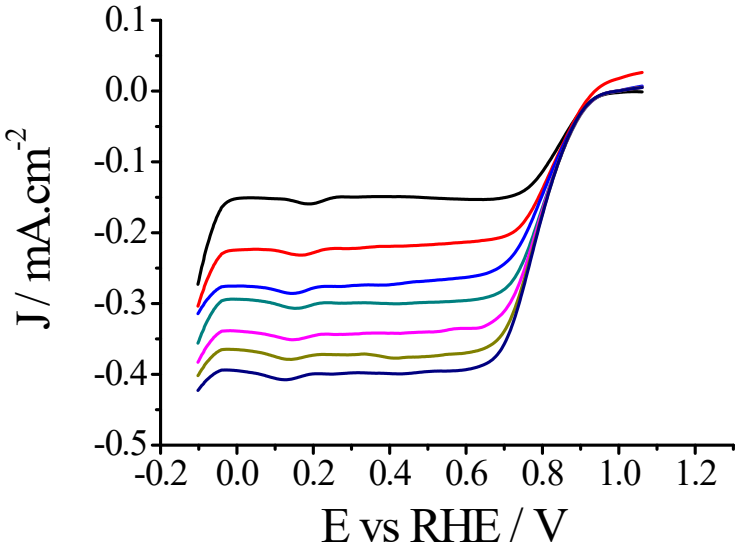

Fig. S15. RDE voltammetric curves in O_2-saturated 0.1 M KOH solution of GC disk electrodes modified with commercial Pt/C. ω = 400, 600, 900, 1200, 1600, 2000 rpm.

For comparison, electrochemical experiments were also performed on commercial Pt/C (Aldrich) in the same conditions as we performed the other experiments on calix-AgNPs and citrate-AgNPs. In these conditions, we found for Pt/C onset potential and half-wave potential equal to 0.92 V and 0.78 V vs RHE respectively. Surface activity calculated at 0.75 V vs RHE is equal to 3.42 $mA.cm^{-2}$. Interestingly, one can note that the maximum current density (plateau current) is nearly 10 time lower than the one obtained for 6 nm calix-AgNPs.

Table S1. Electrocatalytic parameters for ORR reported for silver electrocatalysts.

Catalyst	Electrolyte	E_{onset}, $E_{1/2}$ V vs RHE	Tafel Slopes mV.dec^{-1}	J_K, J_{Ksp} (mA.cm^{-2}) J_M (A/g)	n	Ref
Pt(20 %)/C	1 M NaOH	nd, ≈0.95	50	nd	3.7	[11]
Pt/ Vulcan	0.1 M KOH	nd, ≈0.89	81	nd	3.9	[12]
Polycristalline Ag	0.1M NaOH	0.87, nd	nd	nd	3.2 @ 0.37V	[13]

AgNPs(4.5nm) [a]		0.87, nd	nd	nd	3.7 @ 0.37V	
AgNCs (37nm) [a] **AgNDs (35nm)** [a]	0.1M KOH	0.89, nd 0.89, nd	nd nd	nd nd	3.2 @ 0.37V 3.8 @ 0.37V	14
Ag-A (38nm) [b] **Ag-K (62nm)** [c] **Ag-KC (113 nm)** [d]	0.1M NaOH	≈ 0.83, nd ≈ 0.78, nd ≈ 0.78, nd	nd nd nd	nd, 0.45, 18.9 @ 0.73V nd, 0.74, 25.9 @ 0.73V nd, 0.70, 4.2 @ 0.73V	3.8 @ 0.43V 3.6 @ 0.43V 3.5 @ 0.43V	15
Ag/GO/C [e] **(13nm)** **Ag/GO (13nm)**	0.1M NaOH	0.83, 0.7 0.7, 0.56	nd nd	nd nd nd	nd nd nd	16
Polycristalline Ag	1M NaOH	nd, nd	94, 108	nd	nd	17
Pulse laser deposited (PLD) Ag (<5nm)	0.1M KOH	≈0.85, 0.66	79 , 138	nd, 0.32, 26.7 @ 0.85V	nd	18
Porous PLD Ag (50-200nm)	0.1M KOH	1, 0.86	nd	nd, nd	3.9 - 4	19
Bare AgNRs (83nm) **Ag NRs with PVP (83nm)**	0.1M KOH	≈0.67, 0,60 ≈0.57, 0.51 (plateau 1)	nd nd	13, nd, 92 @ 0.43V 4.17, nd, 29 @ 0.44V (plateau 1)	3.9 @ 0.43V 2.6 @ 0.44V	20
40 wt% Ag/C (10nm) **392 wt% Ag/C (10nm)**	1M KOH (80°C)	0.76, 0.52 0.85, 0.53	62, 118 66, 124	nd, nd nd, nd	3.7 @ 0.4 - 0V 2.6 @ 0.4 – 0V	21
Ag NCs (45 nm) **Ag NPs (18 nm)**	0.1M NaOH	≈ 0.72, 0.57 ≈ 0.72, 0.57	60, 120 60, 120	nd, 0.51 @ 0.72V nd, 0.41 @ 0.72V	nd nd	22
Ag/MWCNT	0.1M KOH	0.95, ≈0.75	80, nd	nd, 0.21 @ 0.72 V	nd	23
Ag-PANI-PVP1 (120nm)	0.1M KOH	0.89, nd	nd	nd	nd	24
AgNClusters (0.7nm) **AgNPs (3.3 nm)**	0.1M KOH	0.87, nd 0.72, nd	nd nd	12.48 1.36	2.3 @ 0.3 – 0.1V 2.8 @ 0.3 – 0.1V	25
AgNPs (2.4nm) [f] **AgNPs (4.6nm)**	0.1M KOH	nd, 0.769 nd, 0.768	nd	nd, 0.0175, 5.3 @ 0.9V nd, 0.021, 4.6 @ 0.9V	nd	9

AgNPs (6nm) **AgNPs (30nm)**		nd, 0.765 nd, 0.722		nd, 0.025, 3.1 @ 0.9V nd, 0.045, 2.6 @ 0.9V		
Bare AgNPs (17nm)	0.1M KOH	≈0.7, ≈0.55	≈ 80	nd, nd	≈ 4	[26]
Calix-AgNPs (6 nm) **Calix- AgNPs (18 nm)**	0.1M KOH	0.74 , 0.50 0.71 , 0.49	≈ 80	2.3, 0.57, 8.09 @ 0.6V 1.4, 0.24, 4.95 @ 0.6V	4 @ full range 3.9 @ full range	This work
Citrate-AgNPs (5nm) **Citrate-AgNPs (20nm)**	0.1M KOH	0.71, 0.47 0.74, 0.50	≈ 80	0.5, nd, 1.77 @0.6V (1.77A/g) 0.57, nd, 2.28 @0.6V	3.7	This work

[a] Synthesized with a ligand which is later removed.

[b] Purchased from Aldrich mixed with Vulcan XC-72 to obtain Ag:C = 60:40 wt%.

[c] Purchased from Kojudo Chemical Lab. mixed with Vulcan XC-72 to obtain Ag:C = 60:40 wt%.

[d] Purchased from Kishida Chemical Co. mixed with Vulcan XC-72 to obtain Ag:C = 90:10 wt%.

[e] Ag deposited on a graphene oxide sheet + addition of Vulcan XC-72.

[f] Synthesized with DDTC which is later removed.

11. Cyclic voltammograms in both O_2 and Ar purged KOH solutions.

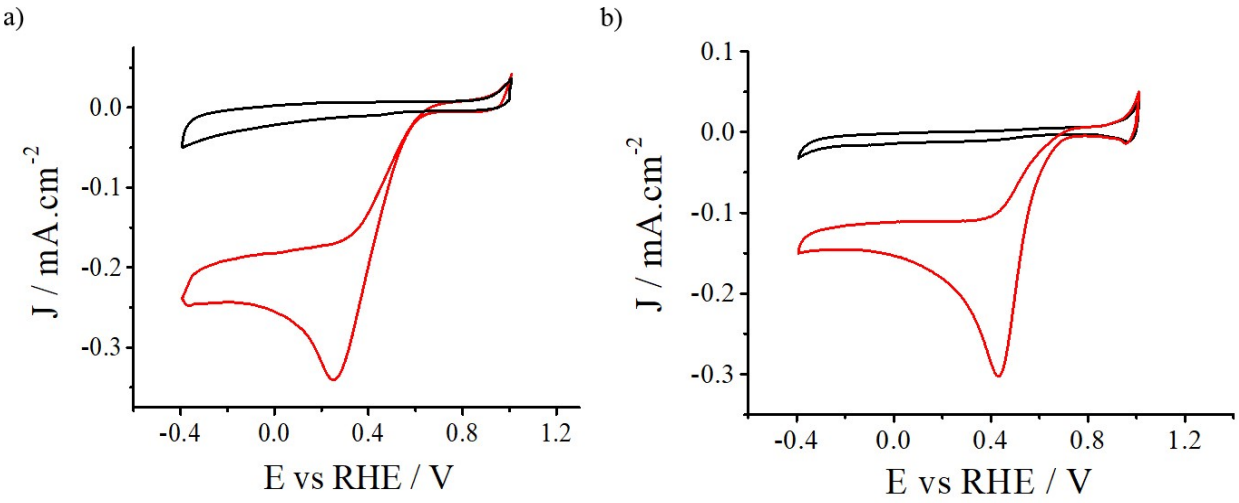

Fig. S16. Cyclic voltammograms in Ar purged (black curves and O_2-saturated (red curves) 0.1 M KOH solution of GC disk electrodes modified a) 6 nm calix-AgNPs and b) 18 nm calix-AgNPs.

12. References.

1. A. Mattiuzzi, I. Jabin, C. Mangeney, C. Roux, O. Reinaud, L. Santos, J.-F. Bergamini, P. Hapiot and C. Lagrost, *Nat. Commun*, 2012, **3**, 1130.
2. L. Troian-Gautier, H. Valkenier, A. Mattiuzzi, I. Jabin, N. V. den Brande, B. V. Mele, J. Hubert, F. Reniers, G. Bruylants, C. Lagrost and Y. Leroux, *Chemical Communications*, 2016, **52**, 10493-10496.
3. M. Retout, I. Jabin and G. Bruylants, *ACS Omega*, 2021, **6**, 19675-19684.
4. S. Zanna, C. Saulou, M. Mercier-Bonin, B. Despax, P. Raynaud, A. Seyeux and P. Marcus, *Appl. Surf. Sci.*, 2010, **256**, 6499-6505.
5. S. Bera, P. Gangopadhyay, K. G. M. Nair, B. K. Panigrahi and S. V. Narasimhan, *J. Electron Spectrosc. Relat. Phenom.*, 2006, **152**, 91-95.
6. G. Schön, J. Tummavuori, B. Lindström, C. R. Enzell and C.-G. Swahn, *Acta Chem. Scand.*, 1973, **27**, 2623-2633.
7. H. Erikson, A. Sarapuu and K. Tammeveski, *ChemElectroChem*, 2019, **6**, 73-86.
8. R. G. C. Fallyn W. Campbell, *Int. J. Electrochem. Sci.*, 2010, **5**, 407-413.
9. S. M. Alia, K. Duong, T. Liu, K. Jensen and Y. Yan, *ChemSusChem*, 2012, **5**, 1619-1624.
10. C. C. L. McCrory, S. Jung, J. C. Peters and T. F. Jaramillo, *J. Am. Chem. Soc.*, 2013, **135**, 16977-16987.
11. J. Perez, E. R. Gonzalez and E. A. Ticianelli, *Electrochimica Acta*, 1998, **44**, 1329-1339.
12. R. Jäger, E. Härk, P. E. Kasatkin and E. Lust, *Journal of The Electrochemical Society*, 2014, **161**, F861-F867.
13. P. Singh and D. A. Buttry, *The Journal of Physical Chemistry C*, 2012, **116**, 10656-10663.
14. Q. Wang, X. Cui, W. Guan, L. Zhang, X. Fan, Z. Shi and W. Zheng, *J. Power Sources*, 2014, **269**, 152-157.
15. J. Ohyama, Y. Okata, N. Watabe, M. Katagiri, A. Nakamura, H. Arikawa, K.-i. Shimizu, T. Takeguchi, W. Ueda and A. Satsuma, *Journal of Power Sources*, 2014, **245**, 998-1004.
16. L. Yuan, L. Jiang, J. Liu, Z. Xia, S. Wang and G. Sun, *Electrochimica Acta*, 2014, **135**, 168-174.
17. S. Kandaswamy, A. Sorrentino, S. Borate, L. A. Živković, M. Petkovska and T. Vidaković-Koch, *Electrochimica Acta*, 2019, **320**, 134517.
18. X. Wu, F. Chen, N. Zhang, Y. Lei, Y. Jin, A. Qaseem and R. L. Johnston, *Small*, 2017, **13**, 1603387.
19. X. Zhao, Z. Deng, W. Zhao, B. Feng, M. Wang, M. Huang, L. Liu, G. Zou, Y. Shao and H. Zhu, *Nanoscale*, 2020, **12**, 19413-19419.
20. Y. Lu, Y. Wang and W. Chen, *J. Power Sources*, 2011, **196**, 3033-3038.
21. X. Xu, C. Tan, H. Liu, F. Wang, Z. Li, J. Liu and J. Ji, *Journal of Electroanalytical Chemistry*, 2013, **696**, 9-14.
22. C.-L. Lee, Y.-L. Tsai, C.-H. Huang and K.-L. Huang, *Electrochem. commun.*, 2013, **29**, 37-40.
23. L. Tammeveski, H. Erikson, A. Sarapuu, J. Kozlova, P. Ritslaid, V. Sammelselg and K. Tammeveski, *Electrochem. commun.*, 2012, **20**, 15-18.
24. U. Stamenović, N. Gavrilov, I. A. Pašti, M. Otoničar, G. Ćirić-Marjanović, S. D. Škapin, M. Mitrić and V. Vodnik, *Electrochimica Acta*, 2018, **281**, 549-561.
25. Y. Lu and W. Chen, *Journal of Power Sources*, 2012, **197**, 107-110.

26. A. Treshchalov, H. Erikson, L. Puust, S. Tsarenko, R. Saar, A. Vanetsev, K. Tammeveski and I. Sildos, *J. Colloid Interface Sci.*, 2017, **491**, 358-366.